

Crystallographic and Electrochemical Characteristics of $\text{La}_{0.7}\text{Mg}_{0.3}\text{Ni}_{4.5-x}(\text{Al}_{0.5}\text{Mo}_{0.5})_x$ ($x = 0-0.8$) Hydrogen Storage Alloys

Xin-Bo Zhang,^[a] Dan-Zi Sun,^[b] Wen-Ya Yin,^[a] Yu-Jun Chai,^[a] and Min-Shou Zhao,^{*[a]}

Keywords: High-rate dischargeability / Low-temperature dischargeability / Exchange current density / Hydrogen diffusion coefficient / Alloys / X-ray diffraction

The structure, hydrogen storage property, and electrochemical characteristics of the $\text{La}_{0.7}\text{Mg}_{0.3}\text{Ni}_{4.5-x}(\text{Al}_{0.5}\text{Mo}_{0.5})_x$ ($x = 0, 0.2, 0.4, 0.6, 0.8$) hydrogen storage alloys have been investigated systematically. The X-ray powder diffraction and Rietveld analysis results reveal that all the alloys mainly consist of the $\text{La}(\text{La}, \text{Mg})_2\text{Ni}_9$ phase and the LaNi_5 phase. The electrochemical measurements show that the maximum discharge capacity increases first from 246.3 ($x = 0$) to 345.4 mAh/g ($x = 0.6$) and then decreases to 317.6 mAh/g ($x = 0.8$), which is consistent with the variation of the hydrogen storage capacity indicated by the P-C isotherms. For the dis-

charge current density of 1200 mA/g, the high-rate dischargeability of the alloy electrodes increases linearly from 47.2% ($x = 0$) to 73.8% ($x = 0.8$). Moreover, according to the linear polarization curves, the exchange current density of the alloy electrodes also increases monotonously with increasing x . The hydrogen diffusion coefficient increases with increasing Al and Mo content, and thus increases the low-temperature dischargeability of the alloy electrodes.

(© Wiley-VCH Verlag GmbH & Co. KGaA, 69451 Weinheim, Germany, 2005)

Introduction

Hydrogen storage alloys have attracted considerable attention in view of their potential as a new energy storage material. Recently, the nickel-metal hydride battery (Ni-MH), in which a hydrogen storage alloy is employed as a negative electrode material, has become the focus of interest as a candidate consumer-used battery by virtue of its several advantages: high reversible energy storage density, high resistance to overcharging and overdischarging, good charge/discharge kinetics, environmental compatibility, and interchangeability with the nickel-cadmium battery.^[1-6] To date, almost all commercial Ni-MH batteries are employing AB_5 -type alloys as negative electrode materials because of their good overall electrode properties.^[7] However, the electrochemical capacity of the AB_5 -type alloys is limited by the single CaCu_5 -type hexagonal structure;^[8] the energy densities of the Ni-MH batteries cannot compete favorably with some other advanced secondary batteries. Therefore, new types of alloys with higher energy densities, faster activation, better rate dischargeabilities, and lower cost are urgently needed to replace the conventional rare-earth-based AB_5 -type alloys.^[9]

Recently, Kadir et al.^[10-12] have reported the discovery of a new type of ternary alloys with the general formula RMg_2Ni_9 (R: rare earth, Ca, Y) with PuNi_3 -type structure. It is found that some of the R-Mg-Ni-based ternary alloys can absorb-desorb 1.8–1.87 wt.-% H_2 , which is much more than the LaNi_5 alloys (which can only absorb 1.4 wt.-% H_2), and are thus regarded as promising candidates for reversible gaseous hydrogen storage.^[13,14] As for their electrochemical hydrogen storage, Chen et al.^[6] have studied the electrochemical characteristics of $\text{LaCaMg}(\text{Ni}, \text{M})_9$ [$\text{M} = \text{Al}, \text{Mn}$] alloys, and almost at the same time, Kohno et al.^[3] have reported that the discharge capacity of the $\text{La}_{0.7}\text{Mg}_{0.3}\text{Ni}_{2.8}\text{Co}_{0.5}$ alloy reached 410 mAh/g. However, up to now, the La-Mg-Ni-Co-system hydrogen storage electrode alloys could not be used as the negative material of the Ni-MH secondary batteries due to their serious corrosion in KOH electrolyte,^[15] and hence their cycling stability had to be upgraded for practical applications. In commercial AB_5 -type alloys, the presence of 10 wt.-% Co has indeed improved the cycling life of Ni-MH batteries. However, it negatively influences the discharge capacity as well as initial activation, and it constitutes about 40% of the material cost.^[16] Much effort has been devoted to search for a more cost-effective substitute element with high reliability of improving the cycling life of Ni-MH batteries. It is believed that Al is one of the best candidates for cobalt substitution.^[17] However, the addition of Al is detrimental to the diffusion of hydrogen from the electrode surface to the alloy bulk, and thus inevitably decreases the high-rate dischargeability of the alloy electrode.^[2] It is reported that the

[a] Key Laboratory of Rare Earth Chemistry and Physics, Changchun Institute of Applied Chemistry, Chinese Academy of Sciences, Graduate School of Chinese Academy of Sciences, Changchun 130022, P. R. China
E-mail: eboat@ciac.jl.cn

[b] State Key Laboratory of Electro-analytical Chemistry, Changchun Institute of Applied Chemistry, Chinese Academy of Sciences, Graduate School of Chinese Academy of Sciences, Changchun 130022, P. R. China

addition of Mo can remarkably increase the kinetic property^[18] as well as the electrochemical capacity of the alloy electrode.^[19] Therefore, it can be expected that the overall electrochemical properties of the La–Mg–Ni-type hydrogen storage alloys could be improved by substitution of Al and Mo for Ni in the alloys.

In this work, on the basis of our previous studies and the belief that the Al and Mo addition may result in some noticeable modifications, the structure and electrochemical characteristics of the $\text{La}_{0.7}\text{Mg}_{0.3}\text{Ni}_{4.5-x}(\text{Al}_{0.5}\text{Mo}_{0.5})_x$ ($x = 0-0.8$) hydrogen storage alloys has been investigated systematically.

Results and Discussion

Alloy Composition and Structure Characteristics

It is well known that the low-melting Mg metal will inevitably be lost during the sample preparation by arc melting. We have tried many ways to overcome this problem, for example, by using an Mg–Ni master alloy as an Mg additive, by decreasing the melting current, by adding a slight excess of Mg over sample composition, and so on. Among all these methods, we found that the latter is the most effective way to compensate evaporative loss of Mg. Several attempts were made until the optimum preparative conditions were found. In this paper, the weight lost during sample preparation is almost the same as excess Mg added. The results of the ICP-AES analysis for all compounds are given in Table 1. It can be seen that the final composition of all the alloys is identical to the original composition.

Table 1. Composition of the $\text{La}_{0.7}\text{Mg}_{0.3}\text{Ni}_{4.0-x}(\text{Al}_{0.5}\text{Mo}_{0.5})_x$ ($x = 0-0.8$) alloys.

Sample	La [mg/g]	Mg [mg/g]	Ni [mg/g]	Al [mg/g]	Co [mg/g]	La:Mg:Ni:Al:Mo ^[a]
$x = 0.0$	263.74	19.78	716.47	0	0	1.90:0.81:12.21:0:0
$x = 0.2$	263.35	19.75	683.61	7.31	25.98	1.90:0.81:11.65:0.27:0.27
$x = 0.4$	262.96	19.72	650.84	14.59	51.89	1.89:0.81:11.09:0.54:0.54
$x = 0.6$	262.56	19.69	618.17	21.86	77.72	1.89:0.81:10.53:0.81:0.81
$x = 0.8$	262.17	19.66	585.59	29.10	103.47	1.89:0.81:9.98:1.08:1.08

[a] Atomic ratio.

The crystal structures have been identified and refined by means of X-ray powder diffraction data. Figure 1 shows the Rietveld refinement pattern of the XRD profiles for the $\text{La}_{0.7}\text{Mg}_{0.3}\text{Ni}_{4.3}(\text{Al}_{0.5}\text{Mo}_{0.5})_{0.2}$ hydrogen storage alloy as a representative example of the $\text{La}_{0.7}\text{Mg}_{0.3}\text{Ni}_{4.5-x}(\text{Al}_{0.5}\text{Mo}_{0.5})_x$ ($x = 0, 0.2, 0.4, 0.6, 0.8$) hydrogen storage alloys. The results show that, besides an impurity Ni phase, the $\text{La}_{0.7}\text{Mg}_{0.3}\text{Ni}_{4.3}(\text{Al}_{0.5}\text{Mo}_{0.5})_{0.2}$ alloy mainly consists of two phases: a La_2MgNi_9 phase with a PuNi_3 -type rhombohedral structure and a LaNi_5 phase with a CaCu_5 -type hexagonal structure. The final Rietveld structure parameters of the La_2MgNi_9 phase are tabulated in Table 2. It can be easily found that the La atoms in La_2MgNi_9 are located not only at the 3a site (the Pu1 atom position of the PuNi_3 structure), but also at the 6c sites (the Pu2 atom position

of the PuNi_3 structure), while the Mg atoms in the alloy exhibit a strong preference for the 6c site, which indicates that the alloy is an ordered compound with the same structure as the previously reported RMg_2Ni_9 ($R = \text{La}, \text{Ca}, \text{Y}$) alloys. Hence, the final formula of the La_2MgNi_9 phase can be designated as $\text{La}(\text{La}, \text{Mg})_2\text{Ni}_9$. The characteristics of the alloy phases in the $\text{La}_{0.7}\text{Mg}_{0.3}\text{Ni}_{4.5-x}(\text{Al}_{0.5}\text{Mo}_{0.5})_x$ ($x = 0-0.8$) alloys are listed in Table 3. We find that all the alloys consist of an impurity Ni phase and two other main crystallographic phases, namely, the $\text{La}(\text{La}, \text{Mg})_2\text{Ni}_9$ phase and the LaNi_5 phase. In addition, variations of the cell parameters and volume of the two main phases as a function of x in $\text{La}_{0.7}\text{Mg}_{0.3}\text{Ni}_{4.5-x}(\text{Al}_{0.5}\text{Mo}_{0.5})_x$ alloys is shown in Figure 2. It can be seen that the parameters a and c of both the $\text{La}(\text{La}, \text{Mg})_2\text{Ni}_9$ phase and the LaNi_5 phase in the alloys increase linearly with an increase in x , which is mainly ascribed to the fact that the atomic radius of Al (1.432 Å) and Mo (1.363 Å) is larger than that of Ni (1.246 Å). Figure 3 shows the abundance of the $\text{La}(\text{La}, \text{Mg})_2\text{Ni}_9$ phase and the LaNi_5 phase as a function of x in the alloys. As can be seen in Figure 3 and Table 3, it can be seen that the $\text{La}(\text{La}, \text{Mg})_2\text{Ni}_9$ phase abundance decreases from 39.21% to 29.79% with increasing x , while the LaNi_5 phase abundance increases from 60.34% to 70.07%. These results may influence the hydrogen storage and electrochemical characteristics of the alloys studied.

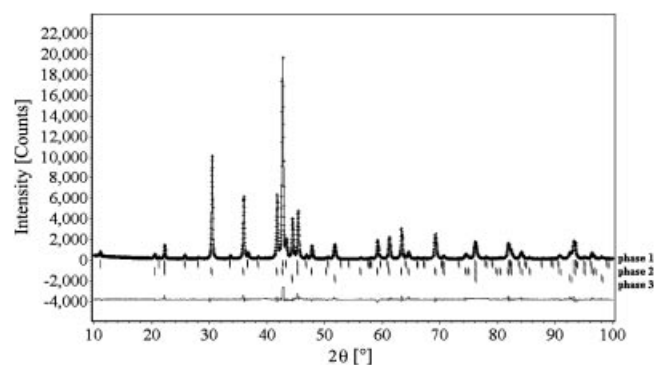


Figure 1. Rietveld refinement pattern of the XRD profiles for the $\text{La}_{0.7}\text{Mg}_{0.3}\text{Ni}_{4.3}(\text{Al}_{0.5}\text{Mo}_{0.5})_{0.2}$ hydrogen storage alloy (Phase 1: $\text{La}(\text{La}, \text{Mg})_2\text{Ni}_9$; phase 2: LaNi_5 ; phase 3: Ni).

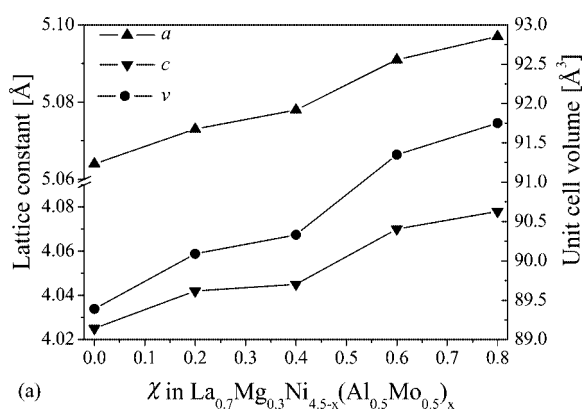
Table 2. Crystallographic parameters for La_2MgNi_9 by using X-ray diffraction $\text{Cu-K}\alpha_1$ ($\lambda = 1.5405981 \text{ \AA}$) at 298 K with a space group of $R\bar{3}m$ and $Z = 3$.^[a]

Atom	Site	Metal atom position			Occupancy
		x	y	z	
La1	3a	0	0	0	1
La2	6c	0	0	0.1427(2)	0.476
Mg1	6c	0	0	0.1427(2)	0.524
Ni1	6c	0	0	0.3311(2)	1
Ni2	3b	0	0	0.5	1
Ni3	18h	0.4996(5)	0.5004(5)	0.0855(6)	1

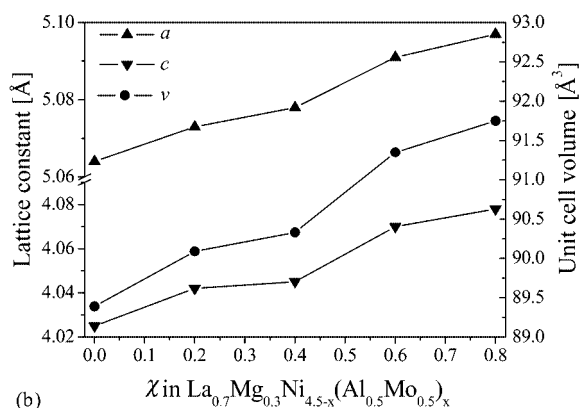
[a] Structure was refined by using the Rietveld refinement program Rietica. The pattern factor is 6.2, the weighted pattern factor is 8.1, and the goodness of fit $S = 2.0$.

Table 3. Characteristics of alloy phases in La_{0.7}Mg_{0.3}Ni_{4.5-x}(Al_{0.5}Mo_{0.5})_x ($x = 0-0.8$) alloys.

Samples	Phases	Phase abundance (wt.-%)	Lattice parameter [Å]			Cell volume [Å ³]
			<i>A</i>	<i>b</i>	<i>c</i>	
$x = 0.0$	La(La, Mg) ₂ Ni ₉	39.21	4.989	4.989	24.093	519.34
	LaNi ₅	60.34	5.064	5.064	4.025	89.39
	Ni	0.45	3.536	3.536	3.536	44.21
$x = 0.2$	La(La, Mg) ₂ Ni ₉	36.85	5.013	5.013	24.369	530.35
	LaNi ₅	62.90	5.073	5.073	4.042	90.09
	Ni	0.25	3.545	3.545	3.545	44.55
$x = 0.4$	La(La, Mg) ₂ Ni ₉	33.59	5.043	5.043	24.410	537.62
	LaNi ₅	65.83	5.078	5.078	4.045	90.33
	Ni	0.58	3.548	3.548	3.548	44.66
$x = 0.6$	La(La, Mg) ₂ Ni ₉	32.41	5.077	5.077	24.622	549.63
	LaNi ₅	67.32	5.091	5.091	4.070	91.35
	Ni	0.27	3.561	3.561	3.561	45.16
$x = 0.8$	La(La, Mg) ₂ Ni ₉	29.79	5.124	5.124	24.713	561.92
	LaNi ₅	70.07	5.097	5.097	4.078	91.75
	Ni	0.14	3.572	3.572	3.572	45.58



(a)

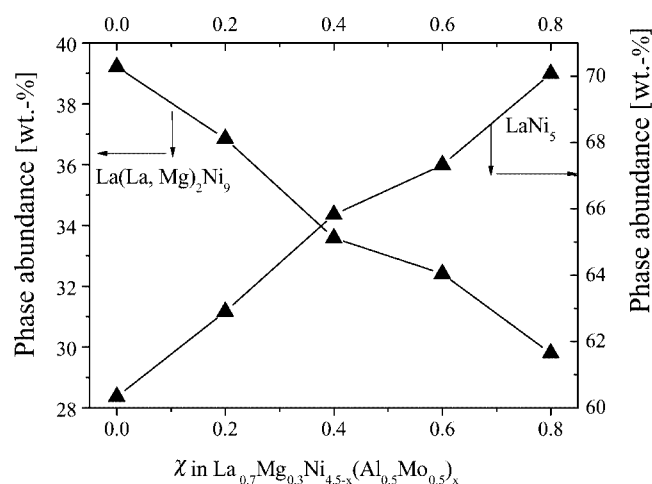


(b)

Figure 2. Variations of the cell parameters and volumes as a function of x in La_{0.7}Mg_{0.3}Ni_{4.5-x}(Al_{0.5}Mo_{0.5})_x alloys ($x = 0-0.8$) (a) La(La, Mg)₂Ni₉ phase; (b) LaNi₅ phase.

P-C Isotherms

The electrochemical pressure-composition isotherm method is very useful for examining the charging and discharging levels of hydrogen in an anode, although the calculated pressures pertain to a quasi-equilibrium state.^[17] Figure 4 shows the electrochemical P-C isotherms for La_{0.7}Mg_{0.3}Ni_{4.5-x}(Al_{0.5}Mo_{0.5})_x ($x = 0-0.8$) alloy electrodes at 298 K. It can be seen that desorption pressure decreases

Figure 3. Phase abundance of the La(La, Mg)₂Ni₉ phase and the LaNi₅ phase existing in the La_{0.7}Mg_{0.3}Ni_{4.5-x}(Al_{0.5}Mo_{0.5})_x ($x = 0-0.8$) alloys.

continually as the addition of Al and Mo increases, which indicates that the stability of the hydrides of the alloys increases with the increasing Al and Mo content. The phenomenon observed here is consistent with those reported previously for AB₃ alloys^[14] and most AB₅ alloys.^[20] Moreover, it can be seen that there is only one plateau in each P-C curve as shown in Figure 4. Since the unit cell of the AB₃ compounds contains one-third of the AB₅ structure and two-thirds of the AB₂ structure,^[6] it is perhaps concluded that the plateau pressure of the La(La, Mg)₂Ni₉ phase is similar to that of the LaNi₅ phase or that the difference between their plateau pressures of the AB₃ and AB₅ compounds is too small to be observed. With regard to the hydrogen storage capacity, it increases from 0.616 to 0.868 wt.-% as x increases from 0 to 0.6. This is mainly attributed to the enhancement of the intrinsic hydrogen storage capacity of the alloy, which results from the decrease in plateau pressure. However, as x increases further, the hydrogen storage capacity decreases to 0.799 wt.-% when x reaches 0.8. This is mainly attributed to the reasons

as follows: it is known that the hydrogen storage capacity of the LaNi_3 phase (1.8–1.87 wt.-% H_2) is larger than that of the LaNi_5 phase (1.4 wt.-% H_2).^[13–14] However, as shown in Figure 3 and Table 3, the $\text{La}(\text{La}, \text{Mg})_2\text{Ni}_9$ phase abundance decreases while the LaNi_5 phase abundance increases with increasing x in the alloys.

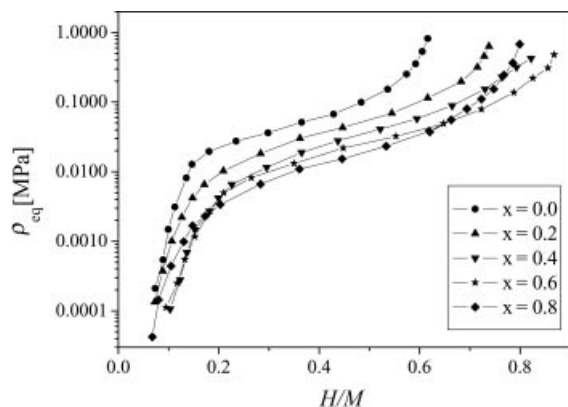


Figure 4. Electrochemical desorption P-C curves for the $\text{La}_{0.7}\text{Mg}_{0.3}\text{Ni}_{4.5-x}(\text{Al}_{0.5}\text{Mo}_{0.5})_x$ ($x = 0, 0.2, 0.4, 0.6, 0.8$) alloys at 298 K.

Discharge Capacity and Discharge Potential

The activation and maximum discharge capacity of the $\text{La}_{0.7}\text{Mg}_{0.3}\text{Ni}_{4.5-x}(\text{Al}_{0.5}\text{Mo}_{0.5})_x$ ($x = 0-0.8$) alloy electrodes are listed in Table 4. It can be seen that all these alloys can be easily activated to reach the maximum capacity within five cycles. The maximum discharge capacity C_{max} improves first and reaches a maximum at $x = 0.6$, and then decreases as x increases further. The variation of the maximum discharge capacity of the alloys is basically consistent with the variation of the H/M with the Al and Mo content in the alloys.

Table 4. Electrode performance of $\text{La}_{0.7}\text{Mg}_{0.3}\text{Ni}_{4.5-x}(\text{Al}_{0.5}\text{Mo}_{0.5})_x$ ($x = 0-0.8$) alloy electrodes.

Sample	H/M	C_{max} [mAh/g]	N_a ^[a]	HRD ₁₂₀₀ ^[b] [%]	S_{70} [%]
$x = 0.0$	0.616	246.3	5	47.2	54.1
$x = 0.2$	0.738	294.8	4	50.6	54.7
$x = 0.4$	0.822	327.6	3	55.8	58.9
$x = 0.6$	0.868	345.4	2	64.7	62.3
$x = 0.8$	0.799	317.6	2	73.8	68.9

[a] The cycle numbers needed to activate the electrodes. [b] The high-rate dischargeability at a discharge current density of 1200 mA/g.

Figure 5 shows the discharge curves (fifth cycle) of the $\text{La}_{0.7}\text{Mg}_{0.3}\text{Ni}_{4.5-x}(\text{Al}_{0.5}\text{Mo}_{0.5})_x$ ($x = 0-0.8$) alloy electrodes at 60 mA/g and 298 K. Obviously, each curve has a wide discharge potential plateau based on the oxidation of desorbed hydrogen from the hydride. Besides, the discharge plateau shifts towards a more positive potential as Al and Mo addition increases in the alloys. As shown in Figure 5,

the mid-discharge potential (potential at 50% depth of discharge) decreases from -0.8710 to -0.8194 V when x increases from 0 to 0.8, which is in good agreement with the reduction of the desorption plateau pressure with increasing Al and Mo content in the alloys.

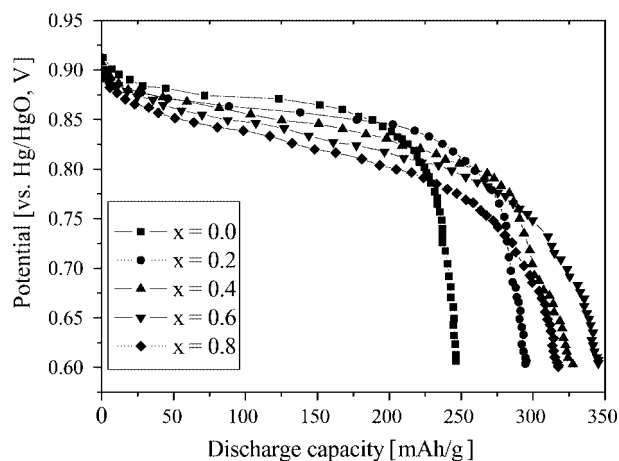


Figure 5. Discharge curves for the $\text{La}_{0.7}\text{Mg}_{0.3}\text{Ni}_{4.5-x}(\text{Al}_{0.5}\text{Mo}_{0.5})_x$ ($x = 0-0.8$) alloy electrodes at the discharge current density of 60 mA/g and 298 K.

Cyclic Stability

The cycling capacity retention rate, expressed as S_{70} (%) = $C_{70}/C_{\text{max}} \times 100$ (where C_{max} is the maximum discharge capacity, C_{70} is the discharge capacity at the 70th cycle), after 70 cycles at 60 mA/g is also listed in Table 4. It can be seen that the capacity retention rate (S_{70}) increases noticeably from 54.1% to 68.9% as x increases from 0 to 0.8, which indicates that the cyclic stability of the La–Mg–Ni–Al–Mo-system alloys is improved markedly with the increase in Al and Mo content in the alloys. It is known that the capacity degradation of the La–Mg–Ni-type alloy electrode results primarily from two factors: the corrosion of Mg and La and the pulverization of the alloy particles.^[20] The Al substitution results in the formation of a protective oxide (hydroxide) of Al on the alloy surface and a subsequent strong protection to the alloy from further corrosion of La and Mg. Moreover, the pulverization of the alloy particles can be improved effectively by substitution of Ni by Mo. In conclusion, the combined effect of the addition of Al and Mo results in the notable increase in the stability of the alloy electrodes. Further investigations in this aspect are going on in our research group.

High-Rate Dischargeability (HRD) and Electrochemical Kinetics

As an important kinetics property of the hydride electrode in batteries, it is very important to restrain the decrease in the discharge capacity even at high discharge cur-

rent density. Figure 6 shows the relationship between the HRD and the discharge current density of the La_{0.7}Mg_{0.3}Ni_{4.5-x}(Al_{0.5}Mo_{0.5})_x ($x = 0-0.8$) alloy electrodes. It can be seen that HRD of the alloy electrodes increases monotonously with increasing x . The HRD of the alloy electrodes at a discharge current density of 1200 mA/g are also listed in Table 4. It can be seen that as x increases, the HRD of the alloy electrodes increases from 47.2% ($x = 0$) to 73.8% ($x = 0.8$). It is well known that the HRD of metal hydride electrodes is influenced mainly by the electrochemical reaction kinetics on the alloy powder surface and the diffusion rate of hydrogen in the bulk of the alloy.^[22] To examine the effect of the partial substitution of Ni by Al and Mo on the discharge kinetics, linear polarization was performed on these alloy electrodes. Based on the measured linear polarization curves, values of the exchange current density I_0 and polarization resistance R_p were evaluated for the alloy electrodes and are summarized in Table 5. Figure 7 shows HRD and R_p as a function of I_0 for the hydrogen evolution reaction at the alloy electrodes. It can be seen that the HRD is a linear function of I_0 . Moreover, we can find that the hydrogen diffusion coefficient (D) remains almost unchanged ($13.1-13.6 \times 10^{-10}$ cm²/s). Iwakura et al.^[23] have pointed out that, if the electrochemical reaction on the surface is the rate-determining factor, a linear dependence of the high-rate dischargeability on the exchange current density should be observed. In contrast, if the diffusion of hydrogen in the bulk is the rate-determining factor, the high-rate dischargeability should be constant, irrespective of ex-

change density. Therefore, in the present study, the HRD is essentially controlled by the charge-transfer reaction of hydrogen on the surface at a discharge current density of 1200 mA/h/g. As the same time, from Figure 7, it can be seen that R_p decreases with increasing exchange current density, while HRD shows the reverse trend, which implies that the R_p value is closely related to HRD.

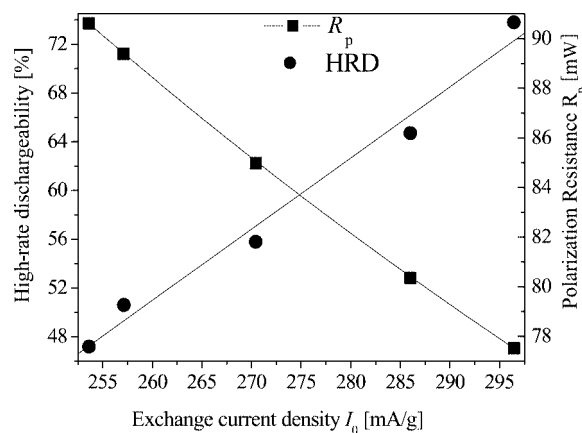


Figure 7. High-rate dischargeability and polarization resistance as a function of exchange current density for hydrogen evolution at La_{0.7}Mg_{0.3}Ni_{4.5-x}(Al_{0.5}Mo_{0.5})_x ($x = 0-0.8$) alloy electrodes.

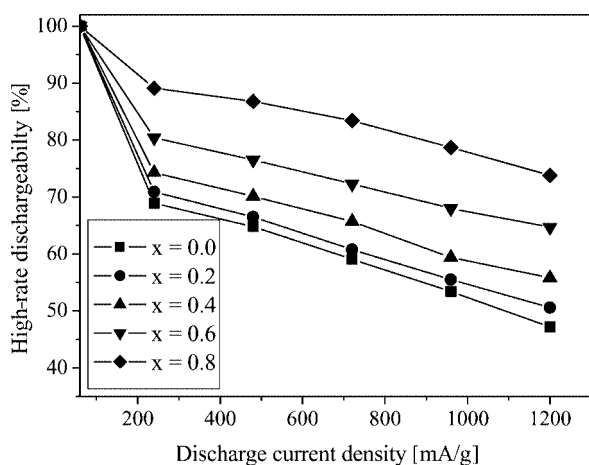


Figure 6. High-rate dischargeability of the La_{0.7}Mg_{0.3}Ni_{4.5-x}(Al_{0.5}Mo_{0.5})_x ($x = 0, 0.2, 0.4, 0.6, 0.8$) alloy electrodes at 298 K.

Low-Temperature Dischargeability (LTD)

It has been reported that the discharge capacity of the negative electrode in nickel-metal hydrides decreases drastically with decreasing temperature.^[24] Sakai et al.^[2] pointed out that the dischargeability of the negative electrodes at relatively low temperatures depended on hydrogen diffusion and/or the charge-transfer process occurring at the metal electrolyte interface. The value of D in the bulk is evaluated using the method described by Iwakura et al.^[18] The LTD is expressed as $LTD_{233} (\%) = C_{233}/C_{298} \times 100$ (where C_{233} and C_{298} are the discharge capacities at 233 K and 298 K, respectively). The values of D and I_0 for the La_{0.7}Mg_{0.3}Ni_{4.5-x}(Al_{0.5}Mo_{0.5})_x ($x = 0-0.8$) alloy electrodes at 233 K are also listed in Table 5. It can be found that both I_0 and D are smaller than that at 298 K. Moreover, we find that I_0 remains almost unchanged (80.35–82.17 mA/g), whereas D increases remarkably with increasing x , which implies that hydrogen diffusion in the alloy probably be-

Table 5. Electrochemical kinetic parameters for the La_{0.7}Mg_{0.3}Ni_{4.5-x}(Al_{0.5}Mo_{0.5})_x ($x = 0-0.8$) alloy electrodes.

Sample	Polarization resistance, R_p [mΩ]		Exchange current density, I_0 [mA/g]		Hydrogen diffusion coefficient, D [$\times 10^{-10}$ cm ² /s]	
	298 K	233 K	298 K	233 K	298 K	233 K
$x = 0.0$	90.61	249.56	253.62	80.35	13.1	1.6
$x = 0.2$	89.38	248.20	257.12	80.79	13.1	3.0
$x = 0.4$	84.98	246.93	270.43	81.21	13.3	3.7
$x = 0.6$	80.36	245.62	286	81.64	13.5	4.8
$x = 0.8$	77.52	244.04	296.45	82.17	13.6	6.2

comes the rate-determining factor for low-temperature dischargeability at 233 K. Figure 8 shows the LTD as a function of D in the alloy electrodes. It can be easily seen that D increases with an increase in x , which can be attributed to cell-volume expansion. The larger the value of D , the greater the LTD of the alloy electrodes.

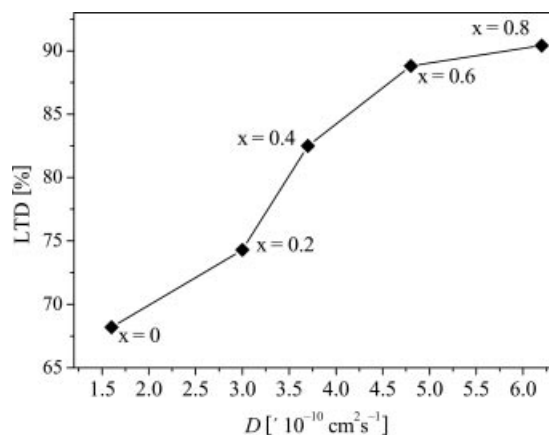


Figure 8. The low-temperature dischargeability (LTD) as a function of hydrogen diffusion coefficient (D) of the $\text{La}_{0.7}\text{Mg}_{0.3}\text{Ni}_{4.5-x}(\text{Al}_{0.5}\text{Mo}_{0.5})_x$ ($x = 0, 0.2, 0.4, 0.6, 0.8$) alloy electrodes at 233 K.

Conclusions

The structure, hydrogen storage characteristics, and electrochemical properties of the $\text{La}_{0.7}\text{Mg}_{0.3}\text{Ni}_{4.5-x}(\text{Al}_{0.5}\text{Mo}_{0.5})_x$ ($x = 0, 0.2, 0.4, 0.6, 0.8$) hydrogen storage alloys have been investigated systematically. It is found that, by X-ray powder diffraction and Rietveld analysis, all the $\text{La}_{0.7}\text{Mg}_{0.3}\text{Ni}_{4.5-x}(\text{Al}_{0.5}\text{Mo}_{0.5})_x$ alloys consist of an impurity Ni phase and two main crystallographic phases, namely, the $\text{La}(\text{La}, \text{Mg})_2\text{Ni}_9$ phase and the LaNi_5 phase. Moreover, the lattice parameters and cell volumes of both the $\text{La}(\text{La}, \text{Mg})_2\text{Ni}_9$ and the LaNi_5 phases increase with increasing Al and Mo content in the alloys. The P-C isotherm curves indicate that the hydrogen storage capacity first increases and then decreases with increasing x , while the desorption pressure always decreases with an increase in x . The electrochemical measurements show that the maximum discharge capacity increases from 246.3 ($x = 0$) to 345.4 mAh/g ($x = 0.6$), and then decreases to 317.6 mAh/g ($x = 0.8$). For a discharge current density of 1200 mA/g, the HRD of the alloy electrodes increases linearly from 47.2% ($x = 0$) to 73.8% ($x = 0.4$). Moreover, according to the linear polarization curves, the exchange current density of the alloy electrodes also increases monotonously with increasing x . The value of D increases with increasing Al and Mo content, and thus increases the LTD of the alloy electrodes.

Experimental Section

Alloy Preparation and X-ray Diffraction Analysis: All alloy samples were prepared by carefully arc-melting the constituent elements on

a water-cooled copper hearth under argon, followed by annealing in vacuo for 100 h at 770 °C. The purity of the metals, i.e. La, Mg, Ni, Al, and Mo is higher than 99.9 mass-%, respectively. The samples were all inverted and remelted 5 times to ensure good homogeneity. A slight excess of Mg over sample composition was needed in order to compensate for evaporative loss of Mg under the preparation conditions. Several attempts were performed to find the optimum preparative conditions. The final compounds were carefully checked by Inductively Coupled Plasma-Atomic Emission Spectrometry (ICP-AES) with a TJA Poems-type instrument. Thereafter, these alloy samples were crushed in a mortar into fine powders of 200–300 mesh.

Crystallographic characteristics of the hydrogen storage alloys were investigated by X-ray diffraction on a Rigaku D/Max 2500PC X-ray diffractometer ($\text{Cu-K}\alpha$ radiation, Bragg–Brentano geometry, 2θ range 10–100°, step size 0.02°, backscattered rear graphite monochromator) by using JADE5 software.^[25] The lattice constants and cell volume were calculated by the RIETICA program after internal θ calibration by using silicon as standard reference material.

Electrochemical Measurement: The alloy powder and carbonyl nickel powder were mixed well in a weight ratio of 1:5 and pressed into tablets as metal hydride electrodes, which had a diameter of 13 mm and a thickness of 1.5 mm; the weight of each electrode was about 0.9 g.

The electrochemical properties were then measured in a standard three-electrode cell consisting of a working electrode (metal hydride electrode), a counter electrode ($\text{NiOOH}/\text{Ni}(\text{OH})_2$ electrode), and a reference electrode (Hg/HgO electrode). The electrolyte in the cell was a 6 M KOH aqueous solution. Charge and discharge tests were carried out on an automatic galvanostatic system (DC-5). The emphasis of these charge/discharge tests was on the electrochemical capacity and stability of the negative electrode, thus the capacity of the positive electrode plate was designed to be much higher than that of the negative electrode. At 298 K, these experimental cells were first charged at current of 60 mA/g for 7 h followed by a rest for 30 min, and were discharged at the same discharge current density to the cut-off voltage of -0.60 V vs. Hg/HgO .

Pressure-composition isotherm (P-C) curves were electrochemically obtained by converting the equilibrium potential of the metal hydride electrode into the equilibrium pressure of hydrogen on the basis of the Nernst equation by using electrochemical data^[26] as reported in reference.^[27] The equilibrium potential curves were obtained by alternating the following two processes: (1) a pulse discharge of (25 mA/g \times 0.25 h), and (2) a rest period until the potential became almost constant. The equilibrium potential change of approximately 30 mV corresponds to the equilibrium pressure change by one order of magnitude. Since the measured potentials have an error of 1–2 mV, the calculated pressure values are accurate to within 10%.^[27]

The high-rate dischargeability (HRD) was defined by the following formula:

$$\text{HRD} (\%) = C_n \times 100 / (C_n + C_{60})$$

where C_n is the discharge capacities of the alloy electrode at a discharge current of n mA/g ($n = 60, 240, 480, 720, 960, 1200$); C_{60} is the additional discharge capacity measured subsequently at 60 mA/g after C_n was measured.

For investigating the electrocatalytic activity of the hydrogen electrode reaction, the linear polarization curves of the electrode were plotted on a EG&G PARC's Model 273 Potentiostat/Galvanostat station by scanning the electrode potential at the rate of 0.1 mV/s

from -5 to 5 mV (vs. open circuit potential) at 50% depth of discharge at 298 K and 233 K. The polarization resistance R_p can be obtained from the slope of the linear polarization curves. Moreover, the exchange current density (I_0), which is a measure of the catalytic activity of the electrode, was calculated from the slopes of the polarization curves by the following Equation (1),^[17]

$$j_0 = \frac{RT}{FR_p} \quad (1)$$

where R is the gas constant; T is the absolute temperature; F is the Faraday constant; and R_p is the polarization resistance. The potentiostatic discharge technique was used to evaluate the coefficient of diffusion within the bulk of the alloy electrodes. After being fully charged followed by a 30 min open-circuit lay-aside, the test electrodes were discharged with a +500-mV potential-step for 500 s on a EG&G PARC's Model 273 Potentiostat/Galvanostat station, by using the M352 CorrWare electrochemical/corrosion software.

Acknowledgments

This work was financially supported by the National Natural Science Foundation of China (Grant No.20171042).

- [1] J. J. G. Willems, K. H. J. Buschow, *J. Less-Common Met.* **1987**, *129*, 13–30.
- [2] T. Sakai, H. Miyamura, N. Kuriyama, A. Kato, K. Oguro, H. Ishikawa, *J. Electrochem. Soc.* **1990**, *137*, 795–799.
- [3] T. Kohno, H. Yoshida, F. Kawashima, T. Inaba, I. Sakai, M. Yamamoto, M. Kanda, *J. Alloys Compd.* **2000**, *311*, L5–L7.
- [4] J. J. G. Willems, *Philips J. Res.* **1984**, *39*, 1–94.
- [5] H. G. Pan, Y. F. Zhu, M. X. Gao, Q. D. Wang, *J. Electrochem. Soc.* **2002**, *149*, A829–A833.
- [6] J. Chen, N. Kuriyama, H. T. Takeshita, H. Tanaka, T. Sakai, M. Haruta, *Electrochem. Solid-State Lett.* **2000**, *3*, 249–252.
- [7] T. Sakai, I. Uehara, H. Iwakura, *J. Alloys Compd.* **1999**, *293–295*, 762–769.
- [8] J. J. Reilly, G. D. Adzic, J. R. Johnson, T. Vogt, S. Mukerjee, J. McBreen, *J. Alloys Compd.* **1999**, *293–295*, 569–582.
- [9] Y. F. Liu, H. G. Pan, Y. F. Zhu, R. Li, Y. Q. Lei, *Mater. Sci. Eng. A* **2004**, *372*, 163–172.
- [10] K. Kadir, T. Sakai, I. Uehara, *J. Alloys Compd.* **1997**, *257*, 115–121.
- [11] K. Kadir, N. Nuriyama, T. Sakai, I. Uehara, L. Eriksson, *J. Alloys Compd.* **1999**, *284*, 145–154.
- [12] K. Kadir, T. Sakai, I. Uehara, *J. Alloys Compd.* **1999**, *287*, 264–270.
- [13] K. Kadir, T. Sakai, I. Uehara, *J. Alloys Compd.* **2000**, *302*, 112–117.
- [14] J. Chen, H. T. Takeshita, H. Tanaka, N. Kuriyama, T. Sakai, *J. Alloys Compd.* **2000**, *302*, 304–313.
- [15] B. Liao, Y. Q. Lei, L. X. Chen, G. L. Lu, H. G. Pan, Q. D. Wang, *J. Power Sources* **2004**, *129*, 358–367.
- [16] P. H. Notton, P. Hokkeling, *J. Electrochem. Soc.* **1991**, *138*, 1877–1885.
- [17] T. Sakai, H. Miyamura, N. Kuriyama, A. Kato, K. Oguro, H. Ishikawa, *J. Less-Common Met.* **1990**, *159*, 127–139.
- [18] C. Iwakura, H. Senoh, K. Morimoto, Y. Hara, H. Inoue, *Electrochem.* **2002**, *70*, 2–7.
- [19] M. T. Yeh, V. M. Beibutian, S. E. Hsu, *J. Alloys Compd.* **1999**, *293–295*, 721–723.
- [20] J. J. Reilly, “Metal Hydrides Electrodes”, in *Handbook of Battery Materials* (Ed.: J. O. Bessenhard), Wiley, New York, **2000**, pp. 123–127.
- [21] H. G. Pan, Y. F. Liu, M. X. Gao, Y. Q. Lei, Q. D. Wang, *J. Electrochem. Soc.* **2003**, *150*, A565–A570.
- [22] T. Sakai, H. Miyamura, N. Kuriyama, A. Kato, K. Oguro, H. Ishikawa, *J. Less-Common Met.* **1990**, *159*, 127–139.
- [23] C. Iwakura, T. Oura, H. Inoue, M. Matsuoka, *Electrochim. Acta* **1996**, *41*, 117–121.
- [24] H. Senoh, Y. Hara, H. Inoue, C. Iwakura, *Electrochim. Acta* **2001**, *46*, 967–971.
- [25] *Materials Data JADE Realease 5, XRD Pattern Processing*, Materials Data Inc. (MDI), **1997**.
- [26] T. Sakai, K. Oguro, H. Miyamura, N. Kuriyama, A. Kato, H. Ishikawa, C. Iwakura, *J. Less-Common Met.* **1990**, *161*, 193–202.
- [27] H. G. Pan, Q. W. Jin, M. X. Gao, Y. F. Liu, R. Li, Y. Q. Lei, *J. Alloys Compd.* **2004**, *373*, 237–245.

Received: September 28, 2004